Numerical Simulation of Butt Curl in the Semi-DC Casting of Aluminum Slabs

by Nobuhito Ishikawa *

ABSTRACT Butt curl which occurs in the semi-direct chill (DC) casting of aluminum slabs can cause metal bleeding and hot cracking accompanied by coincident bowing that leads to poor yields in slab preparation. To understand the mechanism of butt curl, the author has proprietarily developed a solidification stress model based on the elasto-plastic incremental strain theory involving solidification. The analysis using the model shows that butt curl grows immediately after secondary cooling water begins to impinge on the slab bottom, but its growth rate decreases as the bottom block descends and the slab bottom is cooled increasing in rigidity. It is also shown that the driving force for butt curl growth is the torque moment around the center of the slab bottom, which is caused by the tensile stress generated in the mushy zone along the sump profile.

1. INTRODUCTION

Butt curl, which occurs in the semi-DC casting of aluminum resulting in an upward curling of slab bottoms as shown in Figure 1, can cause defects such as metal bleeding at the short side of slabs, hot cracking of slab bottoms, and slab bending due to the asymmetrical shape of slab bottoms. When it is serious, anyone of these defects can result in a total discard of a slab, thus leading to poor casting yields. Moreover, formation of concave shapes on the short side of slab bottoms referred to as bow requires that the slab has to be severed at the bow position to assure a product width. Accordingly, there is a need for countermeasures that can suppress butt curl to improve casting yields.

Butt curl suppression methods widely used heretofore include the CO_2 method that reduces the efficiency of secondary cooling, the pulse water method, the air turbo method, together with the recent methods of using a mold provided with a secondary cooling water system with two different spray angles, and of using a deep bottom block. However, taking the CO_2 method as an example, it is noted that, because the concentration of CO_2 gas is influenced by ion concentrations in the cooling water, when the water quality is unstable an excessively slow cooling takes place potentially resulting in melting and cracking of the slab bottom. Thus although a set of suitable conditions has to be established in applying the countermeasure technologies mentioned above, it is difficult to generalize these technologies because they belong to technical know-how of each company due to slight differences in their casting facility specifications.

* Technical Research Div., Furukawa-Sky Aluminum Corp.

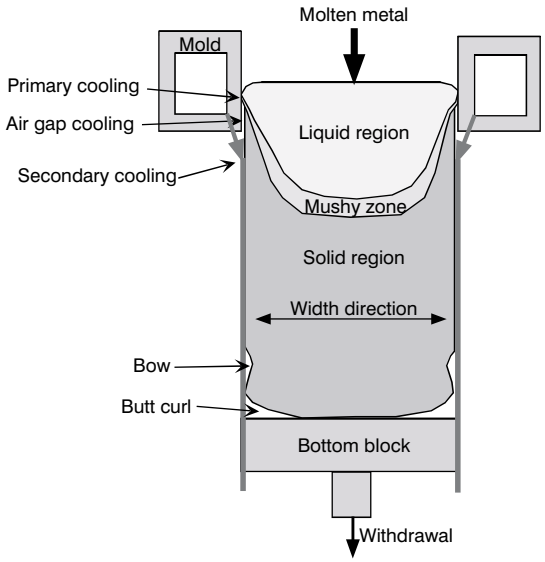

Figure 1 Schematic illustration of aluminum semi-DC casting.

In the study of the mechanism for butt curl generation, Doroste [1] and Tsunekawa [2] made a quantitative measurement of butt curl growth using position sensors cast in slab bottoms, in which they reported that butt curl rapidly grew immediately after secondary cooling water impinged on the slab bottom. Whereas their reports capture the phenomenological essentials of butt curl growth mechanism, they seem to be insufficient in terms of explanation for the solidification stress. Accordingly, the author has developed a solidification stress model based on the elasto-plastic incremental strain theory, in which solidification strains are handled to be definitely different from thermal strains in calculating the process of butt curl growth,

to make comparative evaluations with phenomenological results. In the analysis, the casting process was traced over a withdrawal length of up to 1500 mm from the beginning of casting until the end of butt curl growth, whereby the amount of butt curl was calculated using the data on coordinate variations with respect to the initial (molten) slab shape. In particular, attention was paid to the cooling conditions and temperatures at the initial stage of casting where butt curl rapidly grows, the solidification conditions, and the stress conditions working on the sump profile, thereby making efforts to understand the driving mechanism that govern the process of butt curl growth.

2. THEORY

The solidification stress model developed here combines the temperature model and the stress model of casting taking the temperatures, strains, and stresses during casting into consideration, whereby each model is alternately solved at every calculation time step to hand over the calculated results to the other model. The computational scheme is such that the computational object is a virtual system of molten metal with solid slab in a quarter domain as shown in Figure 2 —which takes into account the symmetry of cast slabs, and that the boundary cooling conditions transfer opposite to the casting direction at the casting speed.

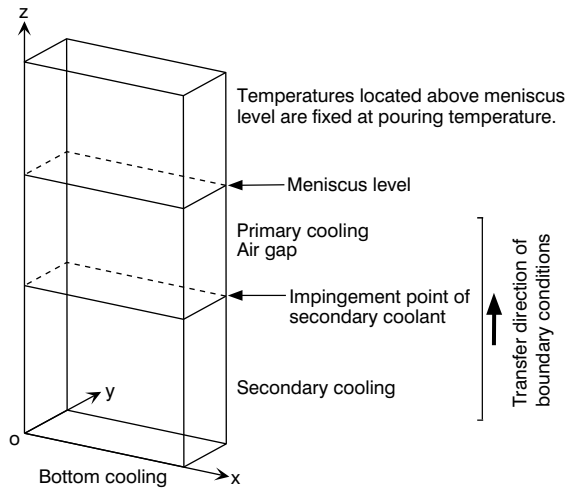

Figure 2 Computational quarter domain in symmetry and boundary conditions.

2.1 Thermal Model

In the calculation of temperatures inside a slab, the temperature recovery method was used taking latent heat into consideration, in which the non-stationary heat conduction equation (Equation 1) is solved excluding the latent heat, and the result is used, after compensated for by a temperature addition corresponding to the latent heat, to redefine the intermediate liquid phase temperature as shown in Equation 2. The increment of solid phase fraction during the course is calculated by Equation 3.

$$\rho C \frac{\partial T}{\partial t} = \kappa \nabla^2 T \tag{1}$$

$$T_{\mathrm{LI}} = T_{\mathrm{L}} - \left(T_{\mathrm{L}} - T_{\mathrm{S}}\right) f_{\mathrm{S}} \tag{2}$$

$$\Delta f_{\mathrm{S}} = \frac{C(T_{\mathrm{LI}} - T)}{L} \tag{3}$$

On the other hand, the surface temperatures of slabs were calculated using the heat transfer equation of Equation 4, in which the heat transfer coefficients for the mold-cooling (primary-cooling) and air-gap cooling regions were given by Equation 5, which enables calculating these coefficients reversely using the measured temperature data on the slab and mold, defining them to be dependent on the air gap. In addition, the heat transfer coefficients for the secondary cooling region were given as a function of the slab surface temperature as shown in Figure 3, which was obtained from temperature measurements of actual slab surfaces and from cooling experiments on high-temperature bottom blocks.

$$\kappa \nabla T = -h\left(T - T_{\infty}\right) \tag{4}$$

$$h = h_{\mathrm{m}} \left(\frac{b}{gap + b} \right)^{c} \tag{5}$$

2.2 Stress Model

In the formula development of stress model, constitutive equations [3), 4)] of the model were derived from the elasto-plastic theory based on the incremental strain theory. In actual calculations, however, the surface force resulting from the head height of molten metal on the sump profile

Nomenclature

B: strain-displacement matrix, C: specific heat, D^{e}: elastic stress-strain matrix, D^{p}: plastic stress-strain matrix, $d\mathrm{S}$: surface element, $d\mathrm{V}$: volume element, f: subsequent yield function, f_{s}: solid phase fraction, G: modulus of transverse elasticity, h: heat transfer coefficient. H': strain hardening coefficient, L: latent heat, T: temperature, T_{ℓ}: liquidus line, T_{s}: solidus line, T_{∞}: boundary temperature

Greek letters

α: linear expansion coefficient, β: solidification shrinkage ratio, Δt: time increment, ε^{e}: elastic strain, ε_{p}: plastic strain, ε^{s}: solidification strain, ε^{T}: thermal strain, $\bar{\varepsilon}^{\mathrm{p}}$: equivalent plastic strain, κ: heat conductivity, Λ: coefficient of normality rule of incremental plastic strain, ρ: density, $\bar{\sigma}$: stress, σ: equivalent stress, σ_{o}: flow stress, σ': deviatoric stress, τ: shear stress, ϕ: shape function of positional coordinate and temperature, ψ: shape function of displacement increment

Greek suffixes denote elements of matrix or vector, and duplicated suffixes in matrix calculation signify summation.

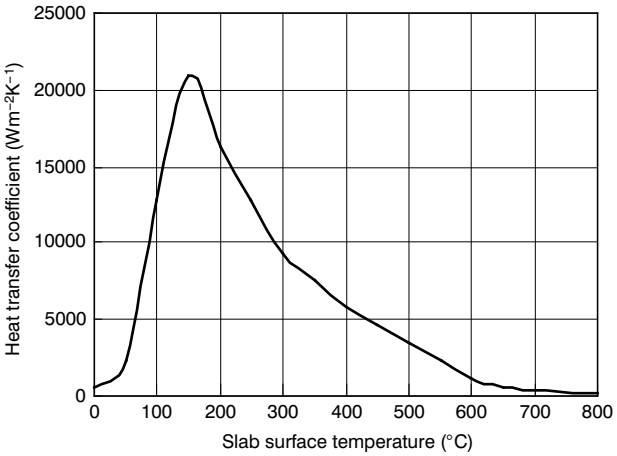

Figure 3 Heat transfer coefficients of secondary cooling.

was ignored due to the fact that the sump is rather shallow in the semi-DC casting of aluminum, together with the volumetric force due to gravity because of its small absolute value in comparison to internal stresses. In the liquid phase region, whereas stress is generated as described later due to the temperature dependency of flow stress, it nearly equals zero since the Young's modulus of the liquid phase appearing in the related formulas is quite small.

It should be noted here that this model excludes both the effect of metal feeding into dendrites and the concept of coherence temperatures [5)~7)] of stresses actually generated.

2.2.1. Constitutive Equation

Based on the incremental strain theory, the total strain increment is defined as a summation of increments of elastic, plastic, thermal, and solidification strains.

$$\Delta\varepsilon_\alpha = \Delta\varepsilon_\alpha^{\mathrm{e}} + \Delta\varepsilon_\alpha^{\mathrm{p}} + \Delta\varepsilon_\alpha^{\mathrm{T}} + \Delta\varepsilon_\alpha^{\mathrm{S}} \tag{6}$$

It was assumed that the thermal and solidification strains were effective only in the solid phase region and the mushy zone, respectively, and that they were isotropic. In particular, the solidification strain expressed by Equation 8 is very important for representing stress concentration [5)] in the mushy zone where butt curl deformation and hot cracking originate from, so that it is thought inadequate to use a simplified formulation where solidification strains are involved with thermal strains.

$$\Delta\varepsilon_{\mathrm{T}} = \left[\alpha\Delta T \quad \alpha\Delta T \quad \alpha\Delta T \quad 0 \quad 0 \quad 0\right]^{\mathrm{T}} \times f_{\mathrm{S}} \tag{7}$$

$$\Delta\varepsilon_{\mathrm{S}} = \left[\beta\Delta f_{\mathrm{S}} \quad \beta\Delta f_{\mathrm{S}} \quad \beta\Delta f_{\mathrm{S}} \quad 0 \quad 0 \quad 0\right]^{\mathrm{T}} \times \left(1 - f_{\mathrm{S}}\right) \tag{8}$$

Next, in order to determine the plastic deformation threshold of a slab, a function type was employed as the subsequent yield function f, which is subject to von Mises yield condition and isotropic hardening rule, using the equivalent plastic strain as a hardening parameter.

$$f(\sigma_\alpha, \bar{\varepsilon}_{\mathrm{p}}, T) = \bar{\sigma} - \sigma_0(\bar{\varepsilon}_{\mathrm{p}}, T) \tag{9}$$

In this connection, since physical properties in the model are assumed to be constant for the sake of simplicity, the dependence on phase transition from liquid phase to complete solid phase is ignored in Equation 9.

By transforming Equation 9 together with Hooke's law of elastic strain, Prager's consistency condition in plastic state, normality rule of incremental plastic strain, and a relational expression between plastic strain and equivalent plastic strain, we can ultimately derive Equation 14, the constitutive equation of the model.

$$\Delta\sigma_\alpha = D_{\alpha\beta}^{\mathrm{e}}\,\Delta\varepsilon_\beta^{\mathrm{e}} \tag{10}$$

$$\Delta f = \frac{\partial f}{\partial \sigma_\alpha}\Delta\sigma_\alpha + \frac{\partial f}{\partial \bar{\varepsilon}_{\mathrm{p}}}\Delta\bar{\varepsilon}_{\mathrm{p}} + \frac{\partial f}{\partial T}\Delta T = 0 \tag{11}$$

$$\Delta\varepsilon_\alpha^{\mathrm{p}} = \Lambda\frac{\partial f}{\partial \sigma_\alpha} \tag{12}$$

$$\Delta\bar{\varepsilon}_{\mathrm{p}} = \left(\frac{2}{3}\Delta\varepsilon_\alpha^{\mathrm{p}}\Delta\varepsilon_\alpha^{\mathrm{p}}\right)^{\frac{1}{2}} \tag{13}$$

$$\Delta\sigma_\alpha = \left(D_{\alpha\beta}^{\mathrm{e}} + D_{\alpha\beta}^{\mathrm{p}}\right)\left(\Delta\varepsilon_\beta - \Delta\varepsilon_\beta^{\mathrm{T}} - \Delta\varepsilon_\beta^{\mathrm{S}}\right) - \frac{1}{S}D_{\alpha\beta}^{\mathrm{e}}\frac{\partial f}{\partial \sigma_\beta}\frac{\partial f}{\partial T}\Delta T \tag{14}$$

Here, the stress-strain matrix D^{p} is a term becoming effective in the plastic state, and can be represented as deviatoric stress shown in Equation 15.

$$D_{\alpha\beta}^{\mathrm{p}} = -\frac{1}{S}D_{\alpha\mu}^{\mathrm{e}}\frac{\partial f}{\partial \sigma_\mu}\frac{\partial f}{\partial \sigma_\nu}D_{\nu\beta}^{\mathrm{e}} = \frac{-1}{\frac{\bar{\sigma}^2 H'}{9G^2} + \frac{\bar{\sigma}^2}{3G}}\begin{bmatrix}\sigma_x'\\ \sigma_y'\\ \sigma_z'\\ \tau_{xy}\\ \tau_{yz}\\ \tau_{zx}\end{bmatrix}\begin{bmatrix}\sigma_x'\\ \sigma_y'\\ \sigma_z'\\ \tau_{xy}\\ \tau_{yz}\\ \tau_{zx}\end{bmatrix}^{\mathrm{T}} \tag{15}$$

It should be pointed out here that even in cases a quadratic form is used for the subsequent yield function, the stress-strain matrix D^{p} thus derived assumes the same formula as Equation 15.

2.2.2. Loading-Unloading Determination

Loading-unloading determination is carried out according to the state of the incremental plastic strain Λ standing on the surface of subsequent yield function as shown below.

In case of f =0 and $\Lambda \geq 0$, then the state of loading:

neutral

In case of f =0 and $\Lambda < 0$, then the state of unloading (16)

Let us note that in the case of subsequent yield function shown in Equation 9, the coefficient Λ equals to the equivalent incremental plastic strain.

3. FINITE ELEMENT FORMULATION

In the finite element formulation of this solidification stress model, isoparametric elements (hexahedron, eight nodal points) are used to represent the position, temperature, and displacement increments in terms of a linear combination of nodal point data and a shape function.

$$X = \phi_\alpha x_\alpha \tag{17}$$

$$T = \phi_\alpha T_\alpha \tag{18}$$

$$\Delta U_\alpha = \varphi_{\alpha\beta} \Delta d_\beta \tag{19}$$

3.1 Finite Element Formulation of Thermal Model

Finite element formulation of the thermal model is carried out by applying the Galerkin method to Equations 1 and 4 to obtain a set of simultaneous equations for every node temperature.

$$C_{\alpha\beta} \frac{\partial T_\beta}{\partial t} + \left(K^1_{\alpha\beta} + K^2_{\alpha\beta}\right) T_\beta = F_\alpha \tag{20}$$

where,

$$C_{\alpha\beta} = \rho C \int \phi_\alpha \phi_\beta \, \mathrm{d}V \tag{21}$$

$$K^1_{\alpha\beta} = \kappa \int \left(\frac{\partial \phi_\alpha}{\partial x}\frac{\partial \phi_\beta}{\partial x} + \frac{\partial \phi_\alpha}{\partial y}\frac{\partial \phi_\beta}{\partial y} + \frac{\partial \phi_\alpha}{\partial z}\frac{\partial \phi_\beta}{\partial z} \right) \mathrm{d}V \tag{22}$$

$$K^2_{\alpha\beta} = h \int \phi_\alpha \phi_\beta \, \mathrm{d}S \tag{23}$$

$$F_\alpha = h T_\infty \int \phi_\alpha \, \mathrm{d}S \tag{24}$$

In terms of time, furthermore, the Crank-Nicolson method is used for discretization to ultimately obtain a finite element formula for the thermal model.

$$\left[\frac{1}{2}\left(K^1_{\alpha\beta} + K^2_{\alpha\beta}\right) + \frac{1}{\Delta t} C_{\alpha\beta} \right] T_\beta \left(t + \Delta t\right) = \left[-\frac{1}{2}\left(K^1_{\alpha\beta} + K^2_{\alpha\beta}\right) + \frac{1}{\Delta t} C_{\alpha\beta} \right] T_\beta (t) + F_\alpha \tag{25}$$

3.2 Finite Element Formulation of Stress Model

Finite element formulation of the stress model is carried out through the principle of virtual work to ultimately obtain simultaneous linear equations in terms of nodal displacement increments, i.e. rigidity equations.

$$\left(K^{\mathrm{e}}_{\alpha\beta} + K^{\mathrm{p}}_{\alpha\beta}\right) \Delta d_\beta = \Delta f^{\mathrm{S}}_\alpha + \Delta f^{\mathrm{V}}_\alpha + \Delta f^{\mathrm{Te}}_\alpha + \Delta f^{\mathrm{Tp}}_\alpha + \Delta f^{\mathrm{Se}}_\alpha + \Delta f^{\mathrm{Sp}}_\alpha + \Delta f^{\mathrm{Y}}_\alpha + \Delta f^{\mathrm{R}}_\alpha \tag{26}$$

The right-hand side comprises the load vectors related with the surface force, volume force, thermal strain, solidification strain, and temperature dependence of flow stress, and the residual term.

$$K^{\mathrm{e/p}}_{\alpha\beta} = \int B_{\mu\alpha} D^{\mathrm{e/p}}_{\mu\lambda} B_{\lambda\beta} \, \mathrm{d}V \tag{27}$$

$$\Delta f^{\mathrm{S}}_\alpha = \int \varphi_{\beta\alpha} \Delta F^{\mathrm{S}}_\beta \, \mathrm{d}S \tag{28}$$

$$\Delta f^{\mathrm{V}}_\alpha = \int \varphi_{\beta\alpha} \Delta F^{\mathrm{V}}_\beta \, \mathrm{d}V \tag{29}$$

$$\Delta f^{\mathrm{Te/p}}_\alpha = \int B_{\mu\alpha} D^{\mathrm{e/p}}_{\mu\lambda} \Delta \varepsilon^{\mathrm{T}}_\lambda \, \mathrm{d}V \tag{30}$$

$$\Delta f^{\mathrm{Se/p}}_\alpha = \int B_{\mu\alpha} D^{\mathrm{e/p}}_{\mu\lambda} \Delta \varepsilon^{\mathrm{S}}_\lambda \, \mathrm{d}V \tag{31}$$

$$\Delta f^{\mathrm{Y}}_\alpha = \int B_{\mu\alpha} D^{\mathrm{e}}_{\mu\lambda} \frac{3\sigma'_\lambda}{2\bar{\sigma} S} \left(-\frac{\partial \sigma_0}{\partial T} \right) \Delta T \, \mathrm{d}V \tag{32}$$

$$\Delta f^{\mathrm{R}}_\alpha = \int \varphi_{\mu\alpha} F^{\mathrm{S}}_\mu \, \mathrm{d}S + \int \varphi_{\mu\alpha} F^{\mathrm{V}}_\mu \, \mathrm{d}V - \int B_{\mu\alpha} \sigma_\mu \, \mathrm{d}V \tag{33}$$

Table 1 Casting conditions and physical properties.

Density (kg/m³)	2500
Heat capacitance (Jkg⁻¹K⁻¹)	1146
Liquidus line (°C)	648
Solidus line (°C)	635
Heat conductivity (Wm⁻¹K⁻¹)	218
Latent heat (J/kg)	3.9×10^5
Thermal expansion coef. (1/°C)	2.5×10^{-5}
Solidification shrinkage ratio	0.07
Slab thickness (m)	0.6
Slab width (m)	1.65
Pouring temperature (°C)	700
Casting speed (mm/min)	60
Secondary coolant flow rate (lcm⁻¹min⁻¹)	3
Heat transfer coefficient in mold region h_m=1400 Wm⁻²K⁻¹, b=0.4, c=0.5 Heat transfer coefficient of secondary cooling Correlation from hot block quenching test	
Node : 1056, Element : 750	

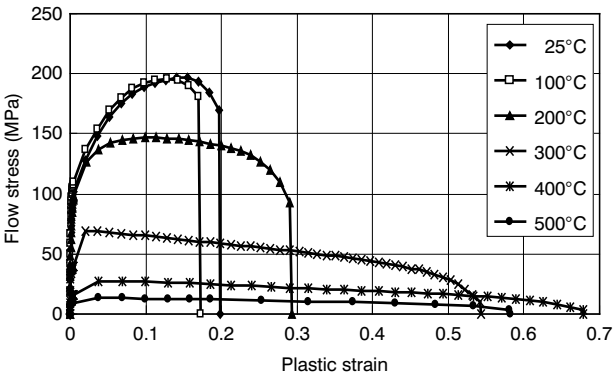

Figure 4 Stress-strain curves of AA3004 aluminum alloy obtained by hot tensile tests.

4. RESULTS OF NUMERICAL CALCULATION

As for the reference conditions for calculating butt curl, casting conditions for an aluminum alloy AA3004 shown in Table 1 were adopted. The initial shape of slab bottom, i.e. the shape of bottom block, was assumed to have double curvatures. The temperature dependence of the flow stress was determined from hot tensile tests in compliance with JIS G0567 as shown in Figure 4, and the flow stress curve was incorporated into the model using the following equation.

$$\sigma_0 \left(T\right) = a\left(T\right) \bar{\varepsilon}_{\mathrm{p}}^{\,n(T)} + \sigma_{\mathrm{y}} \left(T\right) \tag{34}$$

4.1 Process of Butt Curl Growth

In this report, the amount of butt curl is defined as the coordinate variation, due to shape changes, of the short-side center at the slab bottom from its initial position. Figure 5 shows the growth process of butt curl under the reference conditions together with temperature changes during the process at four points on the slab bottom. It

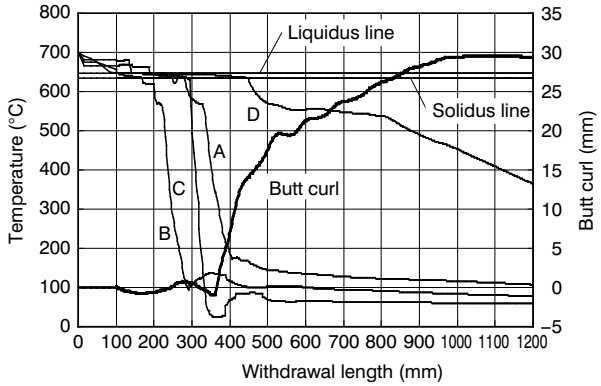

Figure 5 **Calculated temperatures at selected points on the slab bottom and butt curl growth. (A: long side, B: short side, C: corner, D: center)**

can be seen from Figure 5 that, since the withdrawal length on the horizontal axis has a reference point at the center of the slab bottom, impingement of secondary cooling water begins on the short side center at a withdrawal length of 180 mm, and that the water wets the entire periphery at a withdrawal length of 300 mm. It is also seen that butt curl begins to grow rapidly at a 350-mm position where the center portion of the slab bottom starts solidification, gradually decreases in its growth rate as the slab bottom temperature falls, and comes nearly to an end at a withdrawal length of 1000 mm ultimately forming a butt curl of 30 mm.

Figures 6 and 7 show the three-dimensional temperature distributions at the rapid and saturated periods of butt curl growth, and the distributions of vertical stress in the slab width direction (the x-axis direction) that is assumed to be a main source of driving force, respectively. It can be seen that, after the entire periphery of the slab is cooled by the secondary cooling water, the short side of the slab bottom curls up with respect to the initial shape (virtual melt slab) indicated by the frame line, and that bowing occurs simultaneously. In terms of internal stress, a distribution of tensile stress is seen near the sump profile, i.e. mushy zone and high-temperature solid phase region, while compressive stress is generated in the solid phase region around the periphery. The generation of such a stress state is attributable to the feature of the solidification model used here, where the solidification strain is handled to be definitely different from the thermal strain. It would be impossible to obtain the tensile stress distribution clearly shown here along the sump profile if other models are used where the solidification strain is treated as involved with the thermal strain. In this connection, the widespread distribution of tensile stress over the slab bottom appearing at the later stages of descent results from the decreased temperatures in the solid phase region, and it makes little contributions to butt curl growth itself.

The tensile stress distributed near the sump profile is generated by the solidified shell around the periphery where its solidification contraction or thermal contraction being impeded. Conversely, it can be said that the tensile stress near the sump profile pulls the solidified shell

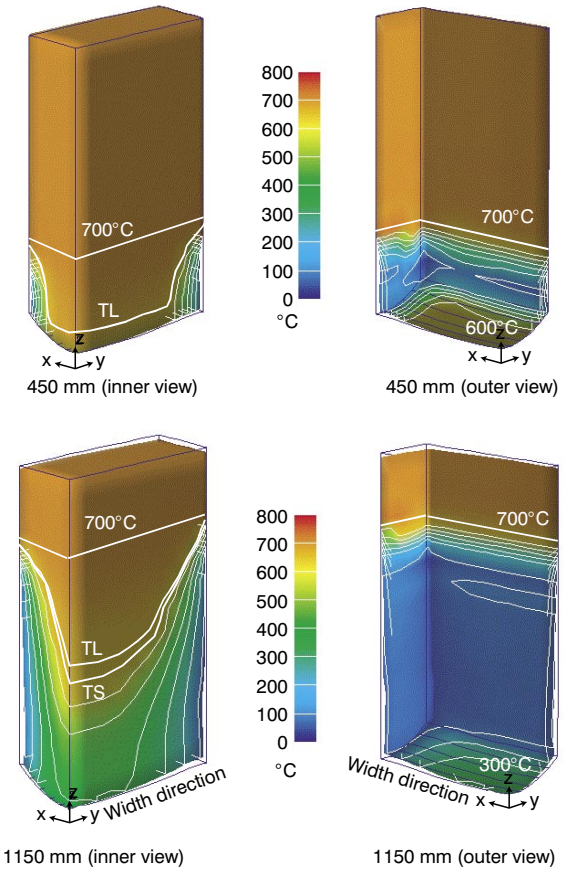

Figure 6 **Calculated temperature distributions at the rapid and saturated periods of butt curl growth.**

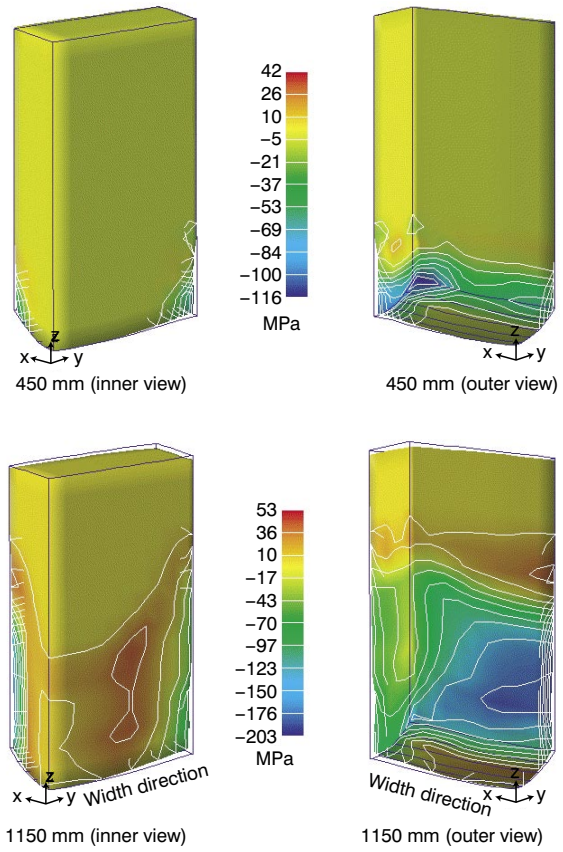

Figure 7 **Calculated vertical stress distributions at the rapid and saturated periods of butt curl growth.**

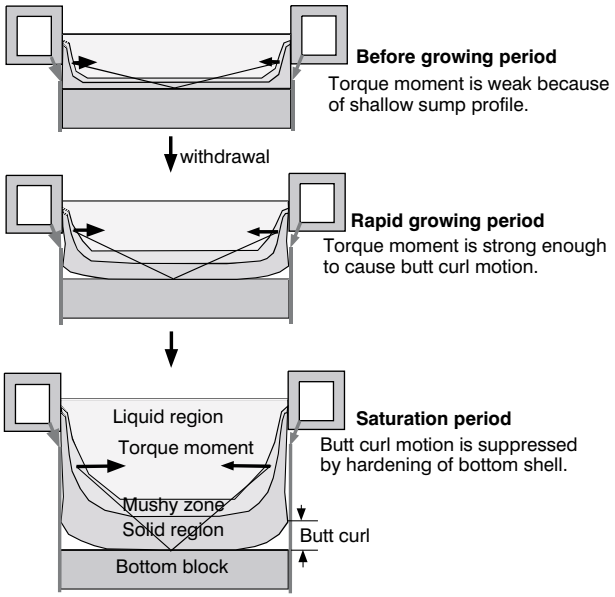

Figure 8 Proposed mechanism of butt curl development: torque moment due to tensile stresses distributed along sump profile bends the solidified bottom shell at the early stage of casting process.

around the periphery toward the inside of the slab. Such a phenomenon may be simulated with several persons forming a circle hand in hand with each other; when they pull their hands all together, they will move toward the center of the circle. Figure 8 illustrates this situation in terms of a torque moment standing on the sump profile, in which it is assumed that this torque moment bends the slab bottom to generate a butt curl. Accordingly, it is thought that while the torque moment is small at the early stage of casting when sump is shallow, it increases as the slab descends leading to the most suitable situation for butt growth where the sump has an appropriate depth and the slab bottom is sufficiently hot yet. When the withdrawal length reaches around 1000 mm, however, the slab bottom presumably increases in size and in rigidity with a decrease in temperature, and it constitutes an obstacle to the torque moment thereby suppressing and terminating butt curl growth.

4.2 Comparison with Butt Curl Measurements

Table 2 shows the casting conditions and butt curl measurements for actual slabs. The samples were selected to have as much a wide variety as possible of casting conditions such as slab width, descent speed, and pouring temperature. Figure 9 shows the results of comparison between the calculated and measured values for butt curl. It is seen that the two values are in good agreement with an accuracy of ±20 %, confirming that the prediction accuracy is superior. In this connection, the temperature dependence of stress-strain curves for each alloy obtained by high-temperature tensile tests is taken into account in this calculation.

4.3 Relationship between Butt Curl and Slab Width

Figure 10 shows the calculated relationship between butt curl and slab width. A linear relationship can be observed

Table 2 Casting conditions and butt curl measurements.

Alloys	Thickness (mm)	Width (mm)	Lowering speed (mm/min)	Pouring temp. (°C)	Measured butt curl (mm)
1xxx	600	1750	50	700	35
1xxx	600	1750	50	700	40
1xxx	600	1280	50	700	22
1xxx	600	1600	63	700	32
3xxx	600	1140	48	690	40
3xxx	600	1140	48	690	35
3xxx	600	1340	60	700	20
3xxx	600	1650	60	700	32
5xxx	600	1920	50	700	30

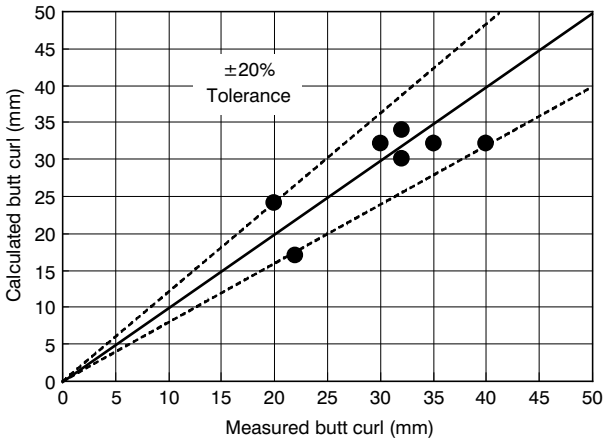

Figure 9 Comparison between calculated and measured values for butt curl.

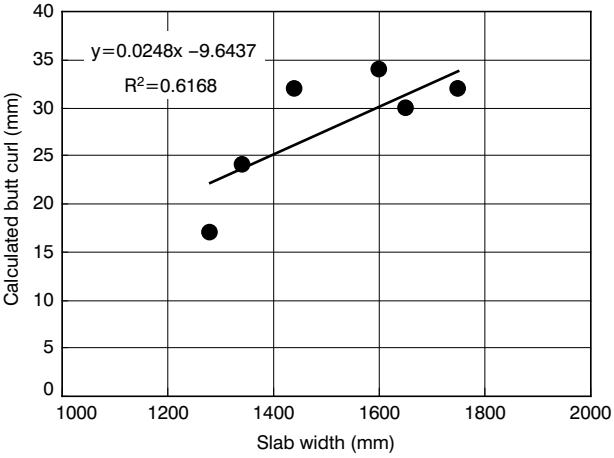

Figure 10 Relationship between butt curl and slab width.

despite a relatively large deviation, and it can be seen that the smaller the aspect ratio (slab width/slab thickness) the smaller the butt curl. The reason for this tendency is presumably that, whereas in general each of the short and long sides of a slab curls up, the internal stress acts to suppress the curl on one side over that on the other side when the latter surpasses the former —just in the case of saddle shape formation in plane bending, so that the smaller the aspect ratio the more these two stresses cancel each other thereby reducing butt curl.

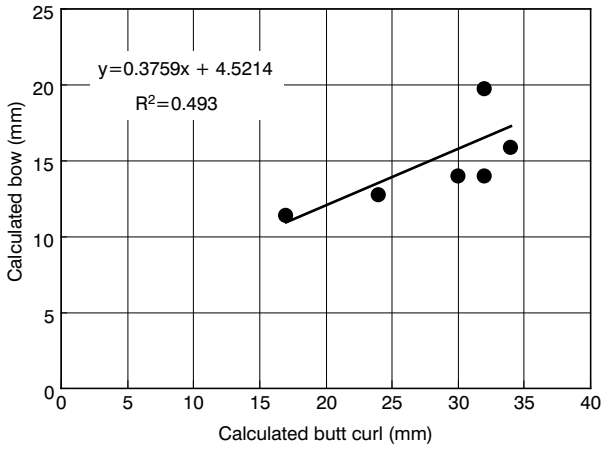

Figure 11 Relationship between butt curl and bow.

4.4 Relationship between Butt Curl and Bow

Figure 11 shows the calculated relationship between butt curl and bow. Here also, a linear relationship can be observed despite a relatively large deviation, and it can be seen that the smaller the butt curl the smaller the bow. It is conceptually understood that the initial rise of a solidified shell on the short side in the form of an integrated L-shaped body naturally leads to bow formation as the shell curls upward, and this mechanism has been adopted by Tsunekawa et al. to explain their experimental results in laboratory. While excessive bowing is known to cause the problem of metal bleeding at the beginning of casting, it is considered that butt curl suppression constitutes the fundamental countermeasures for the problem.

5. CONCLUSIONS

An elasto-plastic solidification stress model has been developed based on the incremental strain theory to analyze the process of butt curl growth. The following conclusions may be drawn from the results:

1) The solidification stress model has been confirmed, through comparison with butt curl measurements, to have an accuracy of prediction of ±20 %, ample performance.
2) In the growth process of butt curl, the torque moment due to the tensile stress acting on the sump profile of the mushy zone plays an important role, and butt curl grows rapidly immediately after the secondary cooling water wets the entire periphery of a slab bottom, and the growth rate decreases to come to an end as the slab bottom decreases in temperature and increases in rigidity.
3) The relationships between butt curl and slab width and between butt curl and slab bow have a tendency similar to that obtained by actual casting.

REFERENCES

1) W. Droste, W. Schneider: Light Metals (1991) 945.
2) M. Tsunekawa, N. Hayashi, T. Uno: Sumitomo Light Metal Technical Reports, Vol.37 (1996) 50.
3) Yagawa and Miyazaki: Analysis of Thermal Stress, Creep and Heat Transfer by Finite Element Method, Science Publishing (1991). (in Japanese)
4) Inoue et al.: Analysis of Solid Physics and Phase Transformation, Okawa Publishing (1995). (in Japanese)
5) Hallvard G. Fjaer, Asbjorn Mo: Metallurgical Transactions B, Vol.21B (1990) 1049.
6) Bruno Hannart, Frederic Cialti, Ruben Van Schalkwijk: Light Metals (1994) 879.
7) Jung-Eui Lee, Tae-Jung Yeo, Kyu Hwan Oh, Jong-Kyu Yoon, U-Sok Yoon: Metallurgical and Materials Transactions A, Vol.31A (2000) 225.